Effect of shear stresses on adenovirus activity and aggregation during atomization to produce thermally stable vaccines by spray drying

Blair A. Morgan[a], Myla Manser[a], Zhou Xing[b], Emily D. Cranston[a,c,d], Michael R. Thompson[a,*]

[a] Department of Chemical Engineering, McMaster University, Hamilton, Ontario, L8S 4L7, Canada

[b] McMaster Immunology Research Centre and Department of Pathology and Molecular Medicine, McMaster University, Hamilton, Ontario, L8S 4L7, Canada

[c] Department of Wood Science, University of British Columbia, 2424 Main Mall, Vancouver, BC, V6T 1Z4, Canada

[d] Department of Chemical and Biological Engineering, University of British Columbia, 2360 East Mall, Vancouver, BC, V6T 1Z3, Canada

[*]Corresponding author: Michael Thompson, mthomps@mcmaster.ca

Abstract

Considering the substantive potential benefits of thermally stable dry powder vaccines to public health, causes for inactivation of their sensitive viral vectors during preparation require intensive study. The focus of this work was atomization of solutions containing encapsulating excipients and a human type 5 adenovirus, involving a detailed investigation of shear stresses in the nozzle of a spray dryer. Samples were sprayed at 25 °C into falcon tubes and immediately evaluated for viral activity by *in vitro* testing, minimizing the confounding of thermal effects on the deactivation of the virus. Despite expectations of only virus deactivation with ever-increasing shear stresses in the spray nozzle, some conditions were found to show better activity than the positive control, leading to investigations of viral aggregation. It was found that the adenovirus experienced minor aggregation when mixed with the excipient solutions, which was reversed by subjecting samples to moderate shear conditions. At very high shear rates, activity diminished again due to damage to the viral capsid, which also led to the production of new aggregates after atomization. Despite these findings, activity losses caused by shear were small compared to the overall spray drying process. However, formulation composition, solution viscosity and process conditions should be considered carefully for medicinal optimization due to their impact on aggregation. This is the first known report comparing shear, aggregation, and biologic activity loss during the atomization step of spray drying thermally stable viral vaccines.

1. Introduction

The immobilization of viruses and viral vectors such as adenovirus, herpes simplex virus, measles virus, and Newcastle disease virus in excipients like mono-, di- and poly-saccharides by spray drying has proven to be promising in preparing vaccines with high thermal stability, minimizing the necessity for adhering to cold chain protocols in maintaining long term efficacy [1–4]. Risk mitigation in spray drying for vaccine manufacture requires an analysis of its unit operations including pumping, atomization, drying, and collection, and evaluating their detrimental effects on the viral vector being stabilized [5]. These unit operations expose any viral vector to thermophysical stresses, growth of the air-liquid interface, and desiccation, all of which are potentially damaging to these sensitive biologics [5, 6]. There are many studies in the literature on damage to enzymes, proteins, and bacteria during spray drying but no guidance on the harmful impact to viruses or viral vectors, which are more sensitive functionally to structural changes [7–9].

The disclosed research is part of a series of studies examining the elementary factors of spray drying influencing the potency of thermally stable vaccines based on adenoviral vectors. Through optimization studies, viral activity was recognized to be dependent on system temperature and spray gas flow rate (and therefore shear) during spray drying, though the scope of prior work did not analyze the factors in detail or attempt to decouple interacting parameters [3, 10]. Subsequently, thermal stresses were examined with the same adenovirus in studies of droplet drying with an acoustic levitator, finding that moderately heated air (30 - 55°C) could actually decrease activity losses [11]. Faster drying, and therefore faster immobilization of the viral vector in a solidified matrix of mixed saccharides, provided earlier thermal shielding compared to unprotected viral vector in liquid exposed to the same ambient conditions. Ultimately, this thermal

shielding was limited since further increasing the air temperature (> 55°C) resulted in viral damage and increased activity losses; thermal stabilization is not boundless by this technology but for viral vectors normally stored at -80°C, even moderate stability well above room temperature is a substantial advancement. This earlier study noted that overall, spray dried powders had larger activity losses than acoustically levitated powders (2.5 log loss higher for a lactose/trehalose formulation and 0.5 log loss higher for a mannitol/dextran formulation) [11].

One major difference between spray drying and acoustic levitation is atomization prior to droplet drying in the former case. Common to pharmaceutical spray drying, atomization involves two impinging fluids, compressed gas and a liquid solution (containing the stabilizing excipients and the viral vector in our case) to produce a fine dispersion of droplets [12]. This subjects the liquid to large shear stresses that are proportional to the feed rates of these two fluid streams and the design of the nozzle [9]. However, looking for specific atomization examples within the spray drying literature shows that little is known about the damaging effects of shear on biologics, with only two relatable cases in which both found the effect to be insignificant [13, 14]. In fact, no examples exist for viruses other than what can be indirectly implied from spray drying optimization studies [3, 10]. The most comprehensive previous study on shear damage of a biologic related to spray drying, found that up to 93% of bacterial death occurring during spray drying of *Lactococcus lactis* and the damage was attributed to shear stresses during atomization by the spray nozzle [9]. Since bacteria are commonly an order of magnitude larger than adenoviruses, making them more prone to high shear stresses based on contact area, these results have little applicability to the present work and their study provided limited information by only investigating three shear rates.

The recognized effects of shear on biologics are conformational changes to enzymes, proteins, and components of the viral capsid, as well as disrupting the RNA/DNA structure of biologics such as viruses and bacteria [7, 15]. Maa and Hsu investigated the effects of shear, or shear combined with increased interfacial area, on the activity of two model proteins using either a concentric-cylinder shear device or a rotor/stator homogenizer in the presence of air [7, 16]. They concluded that denaturation resulted from shear damage and changes to the protein conformation increased due to growth of the air-liquid interface. Levy et al. used two different methods of generating shear stresses to determine their effect on plasmid DNA in solution [15]. Like Maa and Hsu, they concluded that the tertiary structure of DNA could be severely damaged by shear forces, and that the damage was more pronounced when combined with an increase in the air-liquid interface. More specifically for viruses, virus-like particles, and viral surrogates, a small number of studies on shear damage are found in the literature (though not directed to spray drying). Michalsky et al. considered the effect of shear stresses attributed to stirring and pumping but did not observe any change in infectivity of a recombinant baculovirus of *Autographa californica* M nucleopolyhedrovirus [17]. The shear rates in that case were far too low to be comparable to the two-fluid nozzle of a spray dryer, making it difficult to interpret its relevance to the current work. D'Souza et al. used high-pressure homogenization to investigate pressure, shear stresses, and temperature as parameters affecting human enteric virus surrogates, and found up to 3 log loss was obtained, although the effects were not differentiated in their analysis of causes [18].

The objective of the current work was to conduct a detailed investigation on the effects of shear stresses (under 15 different shear conditions) in a spray dryer nozzle on a model viral vector for tuberculosis vaccines, human type 5 adenovirus dispersed in a solution of mono- and poly-saccharides. Since spray drying inherently produces an increase in the air-liquid interface, the

effect of shear will be confounded with this contributing effect in the study. Unexpectedly, in the first stage of the work, we found that adding the viral vector into the mixed saccharide excipient solution led to virus aggregation, but those aggregates could be broken apart at moderate shear;

105 under moderate shear stresses, decreased viral activity loss was observed compared to a non-sheared sample. Higher shear stresses led to increased viral activity loss, possibly caused by structural damage to the viral capsid, which negated the decrease in activity loss caused by de-aggregation. Importantly, the overall damage evident with increased shear stresses was small relative to overall spray drying activity losses, and is likely dependant on both the virus type and

110 formulation being used. These results have implications for both formulation development and scale-up procedures where optimal shear rates can be determined at the lab scale and processing parameters can be adjusted to maintain these shear rates at the industrial scale.

2. Materials and Methods

2.1. Chemicals and adenoviral vector

115 Excipients D-mannitol and dextran (M_r 40,000 kDa) were purchased as USP grades from Millipore-Sigma (Ontario, Canada). Purified water was produced using a Barnstead GenPure Pro water purification system from ThermoFisher Scientific (Waltham, MA) with a resistivity of 18.2 MΩ cm. Life Technologies protocols were used to prepare cell media in-house from α-minimum essential medium (α-MEM) supplemented with 10% fetal bovine serum and 1%

120 streptomycin/penicillin (Invitrogen, Ontario, Canada). A recombinant replication deficient human serotype 5 adenovirus expressing green fluorescent protein (AdHu5GFP) was produced in-house at the vector facility of the McMaster University Immunology Research Center as described previously [19, 20]. The stock viral vector solution consisted of phosphate buffered saline (PBS) with 10% by volume glycerol. Each milliliter of viral stock contains 4.3×10^{12} viral particles, and

125　5.1×10^{10} plaque forming units (pfu). A deactivated AdHu5GFP sample was prepared by exposing 20 µL of stock adenovirus solution to UV light for 45 minutes in a biosafety cabinet. Flow cytometry (as described in Section 2.5) was used to confirm that the virus was deactivated.

2.2. Atomization experiments

　　Trial solutions for the study contained 4% or 8% by weight of an excipient blend at a ratio

130　of 3:1 mannitol:dextran, which was previously found to be highly effective for thermal stabilization of the (non-enveloped) AdHu5GFP viral vector [21, 22]. The viral vector stock solution (10 µL) was added to 10 mL of excipient solution, yielding a viral concentration of 5.1×10^7 pfu. In order to control the shear stresses of atomization under investigation, a B-290 Mini Spray Dryer (Büchi, Switzerland) was used [4, 10, 11]. The spray nozzle (0.7 mm diameter)

135　was operated at room temperature to minimize thermal stresses on the viral vector, and atomized samples were collected directly into 50 mL Falcon tubes while still in liquid form. The characteristic shear rate at the nozzle tip was controlled by adjusting the spray gas feed rate between 282.9 and 1743.7 L/h, and setting the liquid feed rate to 188.5, 290.0, or 440.0 mL/h.

　　For all experiments that did not require viral activity testing, AdHu5GFP was not included

140　in the formulation to minimize vector usage and meet biosafety requirements; since the compositional fraction of the viral was very small (approximately 0.1 wt%) in the formulation, there would be no observable rheological difference in the solution by its absence. The reported data were collected from 3-4 repeated trials, conducted separately by two researchers over a span of several months. Positive controls constituted either a 4% or 8% excipient solution with 10 µL

145　viral vector stock solution added, without any shear applied, hereafter referred to as the "zero shear" samples.

2.3. Excipient solution viscosity

Dynamic viscosities of the excipient blend solutions, at 4% and 8%, were measured using a Discovery Hybrid Rheometer (TA Instruments; New Castle, DE) with a Peltier plate using a 40 mm cone geometry. Testing was done at a controlled temperature of 25°C by a frequency sweep from 0.1 to 5000 rad/s using approximately 0.5 mL of solution.

2.4. Viral aggregation measurements

Viral aggregation was measured using a qViro-X nanoparticle counter (Izon Science; Christchurch, New Zealand) with a NP150 thermoplastic polyurethane membrane with a single nanopore. The analysis range of the NP150 covers particle sizes in the range of 70 to 420 nm (Izon Science; Christchurch, New Zealand). Sheared virus and excipient samples, as well as the "zero shear" samples, were diluted by a factor of five in electrolyte buffer (10 mM HEPES, 150 mM NaCl and 4% by weight sucrose) and tested. The adenovirus control in this case was composed of 10 μL of the viral vector stock solution diluted by addition of 990 μL of electrolyte buffer. All experiments were run with a voltage of 0.46 V applied across the pore. A pressure of 0.6 kPa was applied to the fluid cell using the instrument's variable pressure module to increase the rate of particles passing through the pore. Samples were measured until either 500 events had been recorded or 10 minutes had elapsed. The relationship between blockade event magnitude and particle size was calibrated using CPC100 qNano carboxylated polystyrene calibration beads (Izon Science; Christchurch, New Zealand) with a mean particle size of 115 nm.

2.5. *In vitro* activity testing

In order to minimize potential activity loss during storage, sheared samples were stored on ice and tested on the same day they were produced. 100 μL of a collected sheared sample (excipient

and virus) was mixed with 900 µL of culture media. One well of cultured A549 cells was then incubated with 100 µL of the sample/media mixture overnight, after which point the cells were prepared for flow cytometry. Media was aspirated from the wells and each well was rinsed with 100 µL of PBS. Cells were then trypsinized, and each well was pipetted into a plastic 5 mL round-bottom flow cytometry tube (Corning; Corning, NY) before being centrifuged at 1400 rpm for 5 minutes. The supernatant was discarded and 1 mL of PBS containing 2 mM ethylenediaminetetraacetic acid (EDTA) was added to prevent clumping. The cells were again centrifuged at 1400 rpm for five minutes, the supernatant was discarded, and 1 mL of 1% paraformaldehyde (PFA) was added to each tube to fix the cells. Finally, the cells were centrifuged at 1800 rpm for five minutes, the supernatant discarded, and 200 µL of FACS buffer (0.5% w/v BSA in PBS) was added.

The prepared cells were processed according the Miltenyi Biotec instructions for flow cytometry and run on a MACSQuant Analyzer 10 (Miltenyi Biotec; Bergisch Gladbach, Germany). Data were analyzed using FlowJo software (Tree Star; Ashland, OR): briefly, the autogate function was used to identify the live cell population on of graph of forward scatter versus side scatter in order to reduce variability between experiments. The singlet live cell population was then separated from non-singlet live cells by a user-defined gate on a graph of forward scatter height versus forward scatter area. Finally, the data from a negative control consisting of uninfected A549 cells was gated on a fluorescence histogram graph to split the live, singlet cell population into GFP-positive and GFP-negative. This gate was then applied to all other samples to identify the percentage of the population that was GFP-positive. The percentage of cells expressing GFP was compared against a standard curve using GraphPad Prism (GraphPad Software; La Jolla, CA) to generate a titre value.

2.6. Calculation of characteristic shear rates

The nozzle operates with the excipient solution fed down a central channel by a peristaltic pump with the spray gas fed through a concentric channel around the liquid channel. The mixing zone occurs outside of the nozzle, as shown in Figure 1. External mixing nozzles allow for more control over atomization since both the liquid and spray gas flow rates can be controlled independently [23].
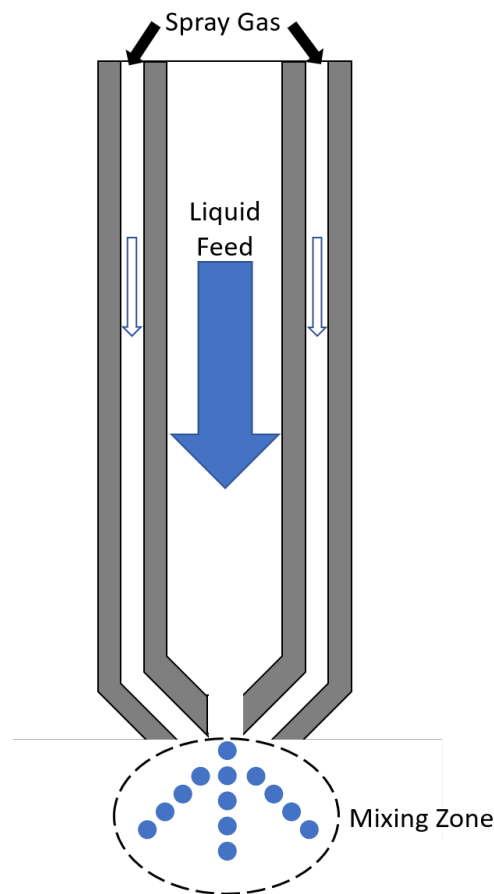
Figure 1: Schematic cross-section of a two-fluid external mixing nozzle such as the one used in this work.

The shear rate in the external mixing nozzle can be estimated as long as only the momentum transfer between the spray gas and liquid feed is considered. If the mass flow rate of liquid in the

nozzle is similar to the mass flow rate of air in the nozzle, as is the case for our experiments using

205   a lab-scale spray dryer, then the average velocity v_{av} (m/s) at the mixing point can be estimated

by Equation 1 [23]:

$$v_{av} = \frac{v_{gas}}{1 + \dfrac{\dot{m}_{liq}}{\dot{m}_{gas}}} \tag{1}$$

where v_{gas} is the velocity of the spray gas at the point of atomization given in units of m/s, and

$\dot{m}_{liq}$ and $\dot{m}_{gas}$ are the mass flow rates of the liquid feed and spray gas, respectively, in units of

210   kg/s. For this calculation, the diameter of the inner nozzle tip was 0.7 mm, while the inner nozzle

cap diameter was 1 mm and the outer nozzle cap diameter was 1.5 mm. The mass flow rates are

calculated by converting the known volumetric flow rates in units of L/h using the density of either

air (the spray gas) or the measured density of the excipient solution. A density of 1.225 kg/m³ was

used for air and a density of 1060 kg/m³ was used as the average of the excipient solution samples.

215   The average density was used to allow for direct comparisons between 4% and 8% solutions,

causing a variation in the shear rate calculation of $\pm 3 \times 10^3$ s⁻¹. Finally, an estimate for the

characteristic shear rate $\dot{\gamma}$ in the spray dryer nozzle was made using Equation 2 [9, 23]:

$$\dot{\gamma} = \frac{2(v_{av} - v_{liq})}{D_i} \tag{2}$$

where D_i is the inner diameter of the nozzle tip (0.7 mm) and v_{liq} is the velocity of the liquid at the

220   point of atomization given in units of m/s. Table 1 shows the spray gas and liquid feed rate settings

used for these experiments and the calculated shear rate values.

Table 1. Characteristic shear rates in the spray dryer nozzle as determined by the spray dryer pump setting and the flow rate of the atomizing spray gas.

		Liquid feed rate (mL/h) [Spray dryer pump setting (%)]		
		188 [13]	290 [20]	440 [30]
Spray gas flow rate (L/h) [Spray dryer setting]	282 [20]	145×10^3 s^{-1}	121×10^3 s^{-1}	97×10^3 s^{-1}
	439 [30]	258×10^3 s^{-1}	225×10^3 s^{-1}	189×10^3 s^{-1}
	666 [40]	433×10^3 s^{-1}	391×10^3 s^{-1}	342×10^3 s^{-1}
	1051 [50]	736×10^3 s^{-1}	686×10^3 s^{-1}	623×10^3 s^{-1}
	1373 [55]	992×10^3 s^{-1}	938×10^3 s^{-1}	868×10^3 s^{-1}

225

2.6. Calculation of aggregate tensile strength

Equation 3 can be used to calculate the force necessary to break up particle aggregates [24]:

$$\sigma = \frac{1.1 \left(\frac{1 - \varepsilon}{\varepsilon} \right) H}{d^2} \tag{3}$$

where σ is the tensile strength of the aggregate (N/m^2), ε is the void volume fraction of the

230   aggregate (unitless), H is the force required to break the bond between individual particles (N), and d is the individual particle diameter (m). In order to calculate the void volume fraction for each, Equation 4 can be used:

$$\varepsilon = \frac{4}{3} \pi \left(\frac{D}{2} \right)^2 - x \left(\frac{4}{3} \pi \left(\frac{d}{2} \right)^2 \right) \tag{4}$$

where D is the diameter of the aggregate given in m, and x is the number of individual particles

235   that make up that aggregate (between two and four in this work).

2.7. Statistical analysis

All sheared samples were used to infect three wells of cells every time activity was evaluated, to assess the variability of the flow cytometry measurements. Quoted uncertainty in the measurements represented the standard deviation of triplicate well infections. Results were

240   statistically analyzed using Microsoft Excel (Microsoft; Redmon, WA) and the Real Statistics

Resource Pack plug-in, where applicable [25]. Viral activity results were considered statistically

significantly different for $p \leq 0.05$ as determined using a one-way analysis of variance with a

Tukey-Kramer Honestly Significant Difference (HSD) post hoc test. For aggregation tests, results

were considered statistically significantly different for $p \leq 0.05$ as determined using a two-sided

245   t-test.

It should be noted that characteristic shear rates of 97×10^3 s^{-1}, 225×10^3 s^{-1}, and

258×10^3 s^{-1} for the 4% formulation were tested separately from other shear rates due to a defect

in the stock viral vector solution used, and that the shear rate of 433×10^3 s^{-1} has been omitted

due to high variability in the activity (the standard deviation was greater than 60% of the mean,

250   which should not be the case for flow cytometry data).

3. Results and Discussion

3.1. Effect of shear rate on viral vector activity

The viral vector AdHu5GFP in a 4% excipient solution of mannitol:dextran (3:1 weight

ratio) was atomized through a spray dryer nozzle (without heat) at 15 different characteristic shear

255   rates, as listed in Table 1. Viral activity of the sheared fluid was reported as titre loss versus shear

rate in Figure 2; throughout these discussions it was a matter of choice to reflect on viral efficacy

based on 'activity loss' rather than 'activity'. The spray gas rate, liquid feed rate and excipient

concentration were selected based on previous spray drying experiments with the same viral vector

[4, 11]. Figure 2 does not show the anticipated monotonic increase in viral titre loss with shear rate

260   demonstrated previously in other works for bacteria but rather, at moderate shear conditions there

was a decrease in activity loss [9]. More specifically, the titre loss decreased from 3.72×10^6 pfu

12

for the "zero shear" sample to a minimum value of 1.55×10^6 pfu ($p < 0.046$) at a shear rate of 391×10^3 s^{-1}, above which the titre loss increased until it levelled off around 2.3×10^6 pfu at higher shear rates. Notably, all shear rates tested had lower activity losses than the "zero shear" sample, implying that shear (within the range tested) had an unexpectedly positive impact on viral activity.

Statistical analysis of data in Figure 2 showed that the titre loss at a shear rate of 391×10^3 s^{-1} was significantly different from the titer losses at 0, 97×10^3, 121×10^3, 225×10^3, 258×10^3, and 686×10^3 s^{-1} (indicated with asterisks over the plotted bars that were statistically different from the minimum which was itself denoted by a # in Figure 2). This verified it was acceptable to consider it a minimum with increases in titre losses on either side of 391×10^3 s^{-1}. Each shear rate condition was repeated 3 to 4 times, and the *in vitro* activity testing was repeated in triplicate for each sample to assess the reproducibility of the methods; the precision is represented by the error bars in Figure 2 and is not identical for all data points but is small compared to the standard deviation values typically shown on log loss plots for activity loss after spray drying [4, 11]. Overall, small variability in the measured titre losses allow us to draw statistically relevant conclusions from the data set and recognize relevant fluctuations that suggest that there are optimal shear conditions that lead to smaller viral activity losses.
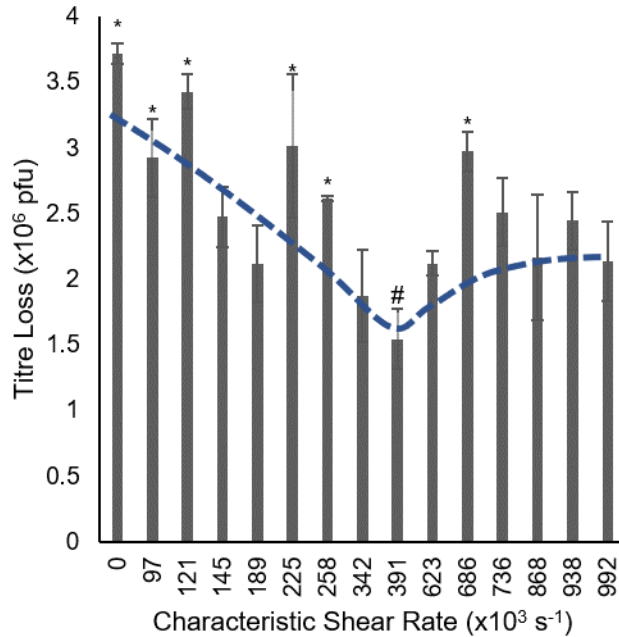
Figure 2: Titre loss of AdHu5GFP after shearing of a 4% mannitol/dextran solution at characteristic shear rates ranging from 97×10^3 to 992×10^3 s^{-1}. Error bars represent standard deviation of triplicate infections from each shear rate. Data points marked with a (*) are statistically significantly different from the data point marked with a (#). The dotted line is a guide for the eye illustrating the trend of viral titre loss and is not based on any regression.

To support the phenomenon seen for AdHu5GFP in the 4% formulation, a more concentrated 8% excipient solution was subjected to the same range of discrete characteristic shear rates. Titre loss as a function of shear rate for the 8% samples is shown in Figure 3. Similar to the results with the 4% solution, viral activity was improved at moderate shear rates compared to the "zero shear" sample. A significant minimum was seen at 258×10^3 s^{-1} ($p < 0.036$), which was lower than the shear rate that corresponded to the smallest activity loss for the 4% formulation. This minimum in titre loss (1.73×10^6 pfu) was statistically different from the losses at tested shear rates of 342×10^3, 391×10^3, 623×10^3, 686×10^3, 736×10^3, and 938×10^3 s^{-1}. With the more concentrated 8% solution, two additional minima were detected at 433×10^3 s^{-1} (p

14

< 0.044) and 992×10^3 s^{-1} ($p < 0.050$), that could not be deemed statistically insignificant. While

almost all titre loss values remained lower than the "zero shear" sample (except at 736×10^3 s^{-1})

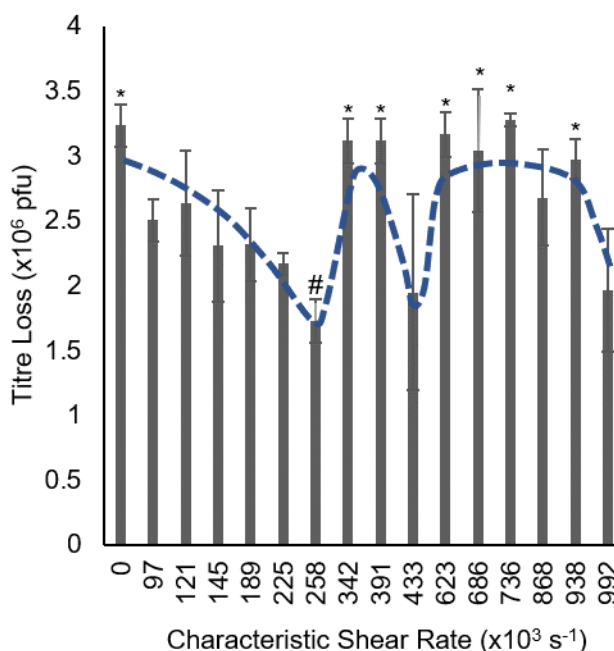the activity losses were higher for 8% formulations compared to 4%.

Figure 3: Titre loss of AdHu5GFP after shearing of an 8% mannitol/dextran solution at

characteristic shear rates ranging from $97 \times 10^3 s^{-1}$ to $992 \times 10^3 s^{-1}$. Error bars represent

standard deviation of triplicate infections from each shear rate. Data points marked with a (*) are

statistically significantly different from the data point marked with a (#). The dotted line is a

guide for the eye illustrating the trend of viral titre loss and is not based on any regression.

Importantly, the shear stresses applied in these experiments led to relatively small activity

losses compared to normal spray drying losses, and under normal operating conditions, shear was

deemed to not significantly impact viral efficacy. We note that the activity results in Figure 2 and

Figure 3 are presented on a linear scale, not the more conventional *log* loss scale, to emphasize the

differences between the various shear rates. If converted to log loss, the values for the sheared 4%

310 formulations ranged from 0.16 to 0.49 log and from 0.18 to 0.45 log for 8%, which are generally

acceptable losses for manufacturing thermally stable vaccines. Compared to the losses expected in

fully spray dried samples (with shear, atomization, heat and drying that are ca. 0.5 to 4 log loss)

these values are small. Only in highly optimized systems have we achieved losses of less than 0.5

log after spray drying with this formulation [10]. As such, even at the highest shear rates tested,

315 viral activity was relatively well-maintained in this study.

From the fluctuations in titre loss measured over the large range of shear rates (and shear

stresses) we infer that several physical mechanisms were affecting viral activity. We hypothesized

that viral aggregates were present in the "zero shear" and lower shear rate samples, causing the

increased activity loss due to a decrease in free non-aggregated viruses available to infect cells. If

320 this aggregation is produced by diluting viral vectors in solutions of mixed saccharides, it would

be a new concern for the field of thermally stable vaccines. Following this hypothesis, the minima

in viral activity loss measured with the 4% and 8% solutions were assumed to be caused by the

break up of these aggregates once a critical shear stress was applied (where the specific shear stress

was related to the size of the aggregate).

325 Superimposed on this aggregation phenomenon, increasing shear stresses had a detrimental

effect on the structural integrity of the viral vector, albeit minor, causing activity losses to increase

after the minima, though only up to a plateau in titre loss. It is reasonable to believe that this

damage occurs in the mixing zone of the nozzle where shear stresses are magnitudes higher than

before or afterwards in the process (Figure 1). Adenoviruses, such as AdHu5GFP used here, are

330 composed of an non-enveloped icosahedral capsid containing genetic information, with elongated

fiber-like proteins extending from each of the 12 vertices of the capsid [26]. These fibers are

responsible for binding to cellular receptors for initiation of the infection process, however are considered very fragile and are the most probable candidates for shear damage in the virus structure [27]. The next section examines the hypothesis of viral aggregation and the effects of shear on de-aggregation.

3.2 Effect of shear rate on viral vector aggregation

Viral particle size was measured using the qViro-X technique for control samples and samples that had been subjected to shear rates of 0, 121×10^3, 391×10^3, and 686×10^3 s^{-1} for 4% formulations, and 0, 121×10^3, 258×10^3, and 686×10^3 s^{-1} for 8% formulations. These samples were chosen so that there would be aggregation data from zero shear up to shear rates encompassing one activity loss minima for each formulation. The cut-off particle size for the measurements was set at 420 nm by the nanopore size of the qViro-X membrane used. Figure 4(a) shows the particle size distributions for the controls: (1) a viral vector stock solution and (2) a UV-deactivated sample of the same viral vector stock solution – neither sample included excipients nor were they sheared. The distributions are overlaid to highlight the difference between an unaggregated and highly aggregated sample. UV deactivation of adenoviruses has been shown to primarily occur due to viral DNA damage; aggregation of the deactivated sample is a likely side effect of the deactivation process caused by adenoviral protein damage [28, 29].

The control stock solution was found to contain particles with a monomodal size distribution, including few aggregates (with sizes larger than 129 nm), giving a mean particle diameter of 99 ± 17 nm. This is consistent with the range of $70 - 100$ nm cited in the literature for primary adenovirus particles, as well as values measured by the same technique [30, 31]. Defining 129 nm as the "cut-off" above which particles are considered aggregated is explained below with Table 2. The near-absence of aggregates in the stock solution matches with previous findings using

355 disc centrifugation [32]. The size distribution of the other control, the UV-deactivated sample, had

a similar monomodal distribution with a broader right-sided shoulder (with a mean of 113 ± 28

nm) and had many more particles larger than 129 nm, i.e., aggregates, than present in the stock

solution. These results were primarily used to validate the use of the qViro-X technique to measure

adenoviral aggregation. Figure 4(b) shows the size distribution of the 4% formulation "zero shear"

360 sample for comparison. The distribution more closely resembles the stock viral solution than the

UV-deactivated sample, but includes more aggregates than the former case. The size distributions

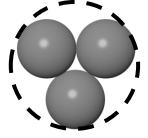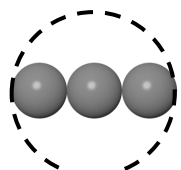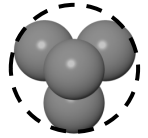for the other seven samples can be found in the Supporting Information, Figures S1 – S7.
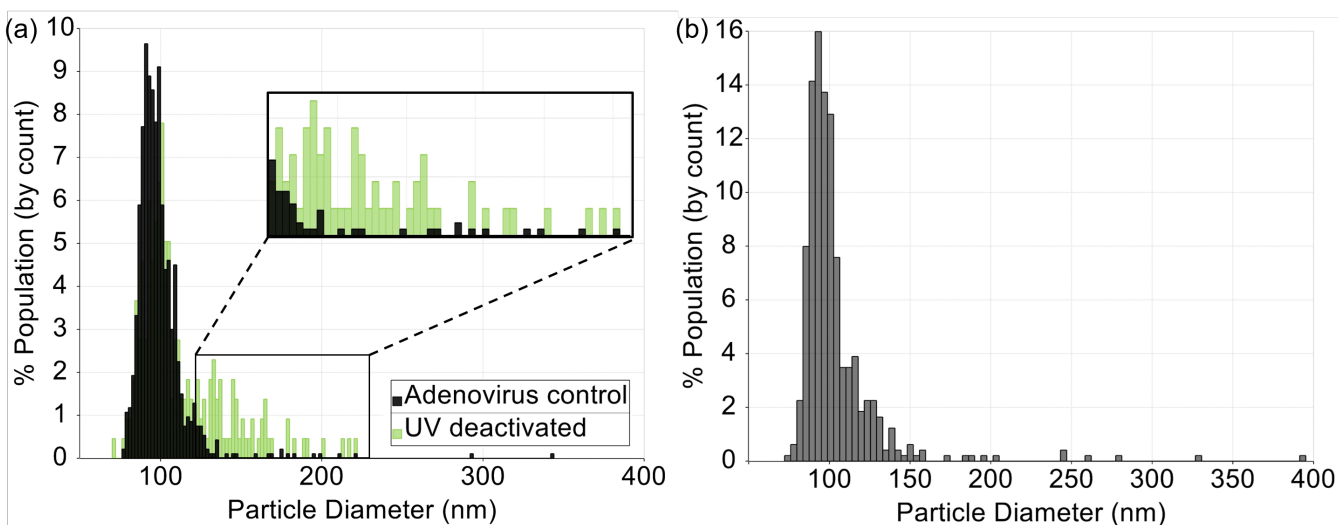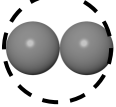
365 **Figure 4:** (a) Comparison of the size distributions for the stock adenovirus control (particle count of 933) and a UV-deactivated virus control (particle count of 218). The stock sample has a main peak of single virus particles with a few larger aggregates; the deactivated sample has a main peak that is centered around a larger diameter, has a large right-sided shoulder, and many more large aggregates. (b) Size distribution of the 4% formulation "zero shear" sample (particle 370 count of 488).

To understand the de-aggregation mechanics and assess whether the changes in number/size of aggregates could explain the decrease in titer loss at certain shear rates during atomization, the possible geometric make-up of viral aggregates first needed to be estimated. The icosahedral shape of the adenovirus can be well approximated by a sphere [33]. Based on this assumption, a radius of gyration (R) could be assigned to aggregates composed of two, three, and four primary viral particles (with radius R_0) following the work of McEvoy et al., who predicted the size of influenza virus aggregates [34]. Aggregate geometry allows the calculation of the void volume fraction, which in turn may be used to estimate the bridge strength between cohesively attached particles. The various aggregates, equations, and calculated diameters were derived using a primary particle diameter of 99 nm and are summarized in Table 2, along with the estimated void volume fraction for each aggregate (Equation 4). The volume-based diameters calculated in Table 2 for suggested available geometries are compared to measured aggregates above 129 nm in Figure 5 for both the 4% and 8% formulation samples; the diameter of 129 nm was selected as the "cut-off" by taking the smallest measured adenovirus diameter (72 nm) and using the dimer formula in Table 2 to calculate the smallest potential aggregate size. Since a primary viral particle may vary between 72-105 nm (Figure 4), the calculated sizes shown in the figure are merely representative of a geometry, we do not believe that the geometries used in this analysis describe all possible aggregate geometries present in the solution. It was simply needed that the measured aggregates and predicted geometries were similar in size in order to later estimate the tensile strength of these aggregates.

Table 2: Equations and calculated volume-based diameters to estimate the size of four different configurations of adenovirus aggregates, as well as void volume fractions (for calculating adenovirus bond strength) calculated using Equation 4. The dotted circles denote the hydrodynamic volumes represented by these geometries.

Aggregate Geometry	Equation*	Calculated Diameter (nm)	Void Volume Fraction

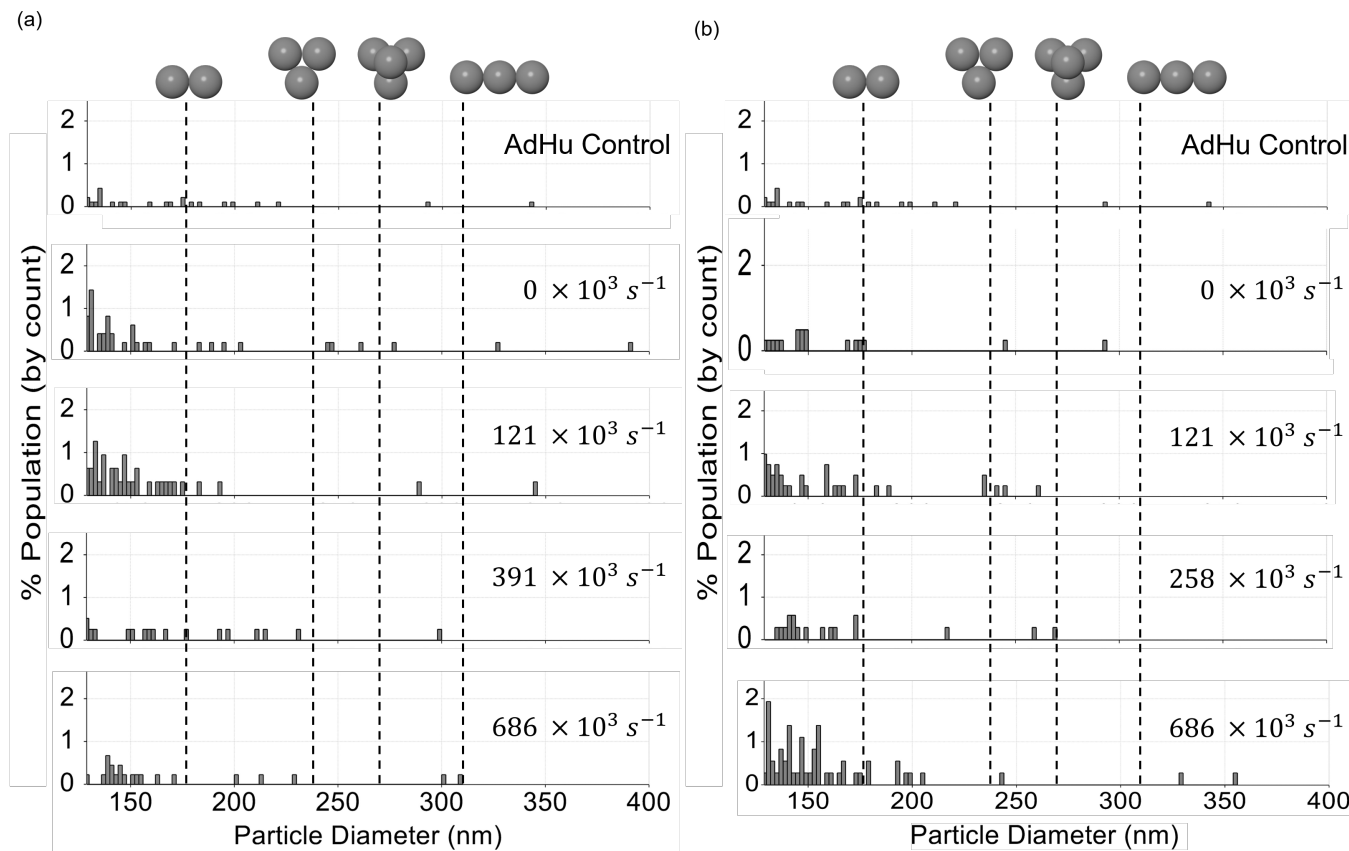|			
Monomer	$R = R_0$	99	-
Dimer	$R^2 = \dfrac{16}{5} R_0^2$	177	0.65
Triangular trimer	$R^2 = \dfrac{29}{5} R_0^2$	238	0.78
Linear trimer	$R^2 = \dfrac{49}{5} R_0^2$	310	0.90
Pyramidal tetramer	$R^2 = \dfrac{37}{5} R_0^2$	270	0.80

* from [34]

Figure 5: Comparison of predicted aggregate diameters with measured adenovirus particle diameters above 129 nm for (a) 4% formulations with no applied shear ("zero shear" sample), an applied shear rate of 121×10^3, 391×10^3, and 686×10^3 s^{-1} (from top to bottom); and (b) 8% formulations with no applied shear ("zero shear" sample), an applied shear rate of 121×10^3, 258×10^3, and 686×10^3 s^{-1} (from top to bottom).

For trials with the 4% formulation, the "zero shear" sample had the highest frequency of large aggregates relative to the stock solution among the sheared samples, as seen in Figure 5(a). These aggregates were a result of the stock solution being added to the solution with excipients. Observed aggregates were largely dimers yet included larger masses consisting of at least three to four adenoviruses like the pyramidal tetramer or linear trimer. As the shear rate was increased from 0, the largest aggregates (close to 400 nm) no longer appeared in the analysis, possibly fractured since they would be the weakest of the particles shown in the figure; at each shear rate, only a

critical aggregate size will persist whereas larger particles will break apart according to Rumpf's

theory for the fracture strength of agglomerated solids [24]. After shearing at 121×10^3 s^{-1}, newer

particle sizes around 340 nm appear that may be related to fracturing of those larger aggregates or

simply other geometric configurations not capable of being broken up at this shear rate. At a shear

415 rate of 391×10^3 s^{-1}, the particle size distribution most closely resembled the control stock viral

solution supporting that the minimum in activity loss at this shear rate for the 4% formulation is

linked to the state of viral aggregation.

However, when the shear rate was increased further to 686×10^3 s^{-1}, the amount of dimer

aggregates present in the 4% formulation increased relative to the sample collected at 391×10^3

420 s^{-1} though the maximum aggregate size remained similar; both the 391×10^3 s^{-1} and the 686×10^3

s^{-1} shear rates had aggregate sizes that suggested both the triangular and linear trimers, but not the

pyramidal tetramer. The production of new (but relatively small) aggregates at 686×10^3 s^{-1} is

thought to be due to removal of the fiber-like proteins on the viral capsid under these shear forces,

allowing for stronger cohesive bridging between viral particles. The shoulder on the distribution

425 at approximately 125 nm is thought to be composed of dimers of viral particles with primary

diameters smaller than 99 nm, or dimers of viral particles without fiber proteins, causing them to

appear smaller than that predicted in Table 2.

For trials with the 8% formulation, all sheared samples and the 'zero shear' sample showed

more aggregation than the control stock solution, as seen in Figure 5(b). Though difficult to make

430 definitive conclusions from the data, it did not appear that there were more or larger aggregates at

this higher excipient concentration in the 'zero shear' sample. This indicates that the concentration

of the excipients at 4% was sufficient to affect the virus population in solution and the higher

concentration produced no new interactions that would lead to further aggregation. As observed

with the 4% formulation, the largest aggregate size decreased in samples by increasing shear from 0 to 121×10^3 s^{-1} while the amount of overall aggregation remained similar between the two operating states. The sample sheared at 258×10^3 s^{-1} (the first minimum in Figure 3) showed the least amount of total aggregation, and had a similar maximum aggregate size to the 121×10^3 s^{-1} sheared sample; the particle size distribution was not as close to the control stock solution as seen for the 4% formulation at the shear rate corresponding to minimum activity loss but the sample did contain considerably fewer aggregates than at other shear condition. The sample subjected to 686×10^3 s^{-1} displayed the most aggregates as well as the largest aggregates for the 8% formulation. Based on the higher shear stresses afforded by its higher solution viscosity, a higher frequency of viruses in this sample were expected to experience damaged capsids, giving the greatest degree of aggregation and deactivation observed.

With only two formulation concentrations studied, we cannot fully model the trend between concentration and the shear rate at which titre loss minima are seen, however, the two-fold increase in concentration from 4% to 8% caused a 1.5-fold decrease in the shear rate that minimized activity loss, suggesting an inverse linear relationship between concentration and minimal shear rate. As the concentration, and therefore viscosity, of the solution increases, it is more likely that damage to the viral structure, and further aggregation, will occur at high shear rates. Therefore, it is recommended to err on the lower end of the applied shear rates during processing, particularly when using more concentrated excipient formulations.

Comparing the particle size distributions in Figure 5 to the titre loss data in Figures 2 and 3, the degree to which viruses were bound in aggregates correlated with higher activity losses. At low or zero shear conditions, the occurring aggregation was attributed to the stock virus solution being mixed with the excipient saccharides. The mean particle diameters (Supporting Information

Table S1) support this finding, showing the samples from both 4% and 8% formulations at "zero shear" had mean particle diameters (104 ± 27 and 103 ± 18 nm, respectively) that were statistically higher than that of the viral stock solution (99 ± 17 nm) ($p < 0.05$). From this we infer that excipient

460 concentration does not appear to significantly affect aggregation and although the cause of 'aggregation due to mixing' is unknown, changes in local ionic strength or pH as the virus and mixed saccharides are brought together may be contributing factors [35]. For both 4% and 8% formulations, the samples showing the least aggregation in Figure 5 (391×10^3 s^{-1} and 258×10^3 s^{-1}, respectively) correspond to an activity loss minima; the lower shear rate for the minima in the

465 8% solution can be attributed to its higher viscosity, indicating the phenomenon was shear stress dependent which would be consistent with an aggregate's fracture strength. Motion through the velocity gradients in the nozzle and mixing zone as the liquid formulation is compressed can increase particle-particle collisions leading to further aggregation and therefore differing aggregate sizes in the sheared samples [32, 33]. The detailed fluid dynamics of the spray dryer nozzle and

470 mixing zone are outside the scope of this work; however, Hede et al. noted that turbulent flow is necessary to break up the liquid flow into droplets [23]. The secondary mechanism for aggregation was attributed to damaged capsids that occurred at higher shear rates. Removal of the viral capsid fiber proteins would allow for closer packing of virus particles, leading to new interparticle bonds and therefore aggregates to be created. These damage-induced aggregates may contribute to the

475 second and third activity minima seen in the 8% formulation as they are broken up.

3.3. Strength of a viral aggregate

Accepting the proposed aggregate geometries above, and the evidence that the minima for titer loss seen with the 4% and 8% formulations corresponded to one or more of these aggregate geometries breaking up, it is possible to estimate the (tensile) fracture strength of these aggregates

24

480   based on the corresponding shear stress when break up occurred. Equation 3 can be rearranged to

calculate H, the interparticle bond strength between two adenovirus particles, giving researchers a

valuable parameter for predicting process conditions that favor de-aggregation. To the best of our

knowledge, this H value has not been reported in the literature previously for adenoviruses. The

estimated value will be limited to adenoviral solutions of comparable viscosity to our formulations,

485   namely 1.1×10^{-3} Pa $\cdot$ s and 1.3×10^{-3} Pa $\cdot$ s, for 4% and 8%, respectively, and displaying

Newtonian behaviour across the range of shear conditions under consideration. The shear rates at

activity loss minima were equated to the break up of aggregate sizes based on their calculated void

volume fractions, with the highest void volume fraction aggregate being considered to fracture at

the lowest shear rate minima and the lowest void volume fraction aggregate fracturing at the

490   highest shear rate minima per formulation.

Table 3 gives the tensile fracture strengths of each aggregate, ordered from lowest to

highest in terms of volume fraction, calculated using the given solution viscosities and shear rates.

The calculated values for the viral interparticle bond strength are all of similar magnitude, between

10 and 33 pN, leading us to conclude that the assumptions above were reasonable. These calculated

495   H values are similar to those reported by Dobrowsky et al. for the strength of adhesion between

HIV surface proteins and cellular receptors, which ranged between 18 and 38 pN [38]. The

difference in calculated bond strength for the linear trimer in the 4% and 8% formulations is small

and within the error of the calculation based on the error in shear rate calculations. As a result of

this analysis, we conclude that 25 pN is a reasonable estimate of the viral bond strength, which

500   should allow researchers to predict the shear rates that correspond to activity loss minima based

on the viscosity of their solutions being spray dried.

Table 3: The tensile strength required to break up each viral aggregate geometry at the various activity loss minima in the 4% and 8% formulations. The tensile strength values were then used to calculate the viral interparticle bond strengths with Equation 3.

Aggregate Geometry (Concentration used in Calculation)	Shear rate @ minima ($\times 10^3 s^{-1}$)	Tensile strength (N/m^2)	Bond strength (pN)
Linear trimer (8%)	258	347	28
Linear trimer (4%)	391	417	33
Pyramidal tetramer (8%)	433	583	21
Triangular trimer (8%)	433	583	18
Dimer (8%)	992	1335	10

505

4. Conclusion

Overall, these data show that there are several mechanisms acting on the virus during the atomization step of thermally stable dry powder vaccine production, impacting both viral activity and aggregation. Initial mild aggregation occurs when the stock adenovirus solution is mixed with excipients, and similarly increased aggregation is seen at higher shear rates caused by damage to the viral capsid, along with increased activity losses. Some of the initial minor aggregation can be reversed by applying moderate shear stresses to the sample, leading to minima in measured activity losses. The exact shear rate at which the most de-aggregation and activity recovery occurs, varies depending on the formulation viscosity, with higher viscosity solutions requiring a lower shear rate to minimize activity loss. While the highest shear rates used in this work caused damage to the viral capsid and an increase in activity loss, the overall effect of shear on adenovirus activity is low compared to conventional spray drying losses and in line with other findings in the literature that shear has little to no effect on the biologic. If optimization during formulation development is possible, the spray gas and liquid feed rates can be tuned based on solution viscosity and viral aggregate tensile strength to minimize viral vector activity.
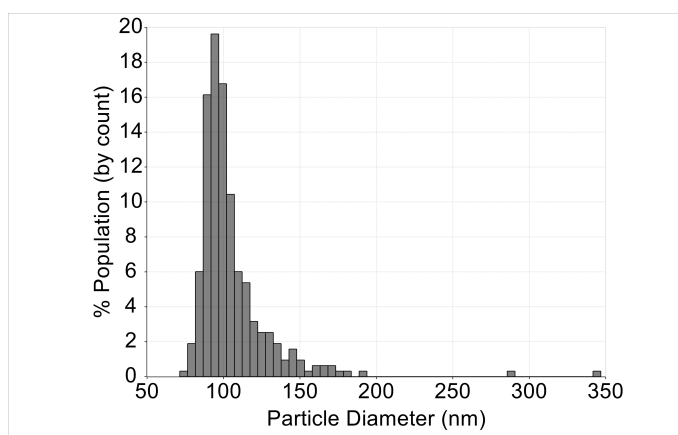
Supporting Information

Figure S1: Size distribution histogram for the 4% sample at a shear rate of 121×10^3 s^{-1}. The particle count for this sample was 316.
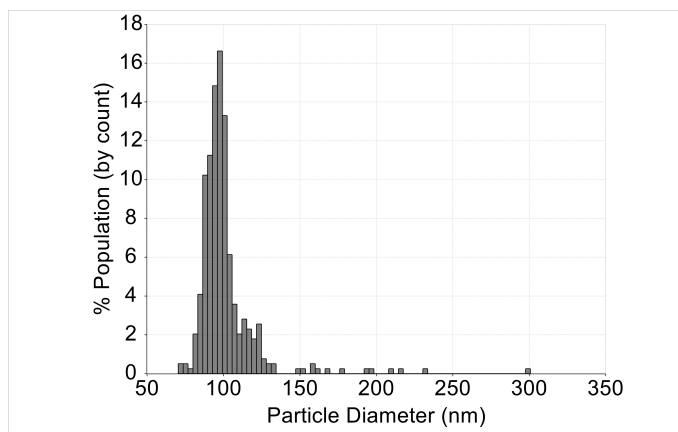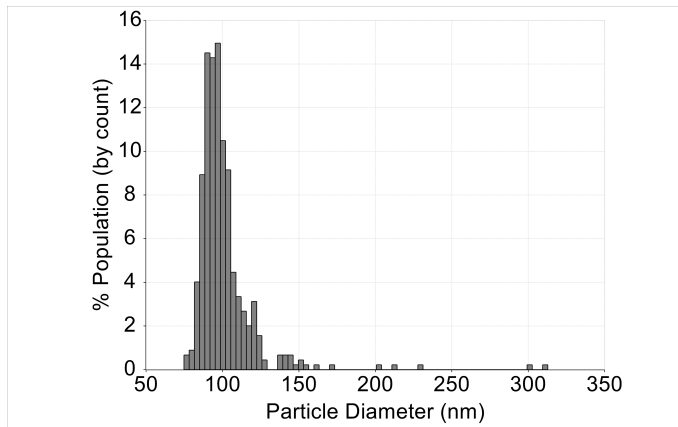
Figure S2: Size distribution histogram for the 4% sample at a shear rate of 391×10^3 s^{-1}. The particle count for this sample was 391.

535   **Figure S3:** Size distribution histogram for the 4% sample at a shear rate of 686×10^3 s^{-1}. The particle count for this sample was 448.

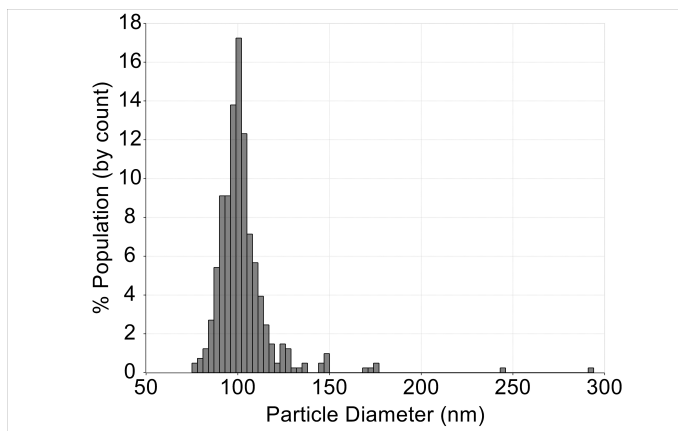**Figure S4:** Size distribution histogram for the 8% "zero shear" sample. The particle count for this sample was 406.
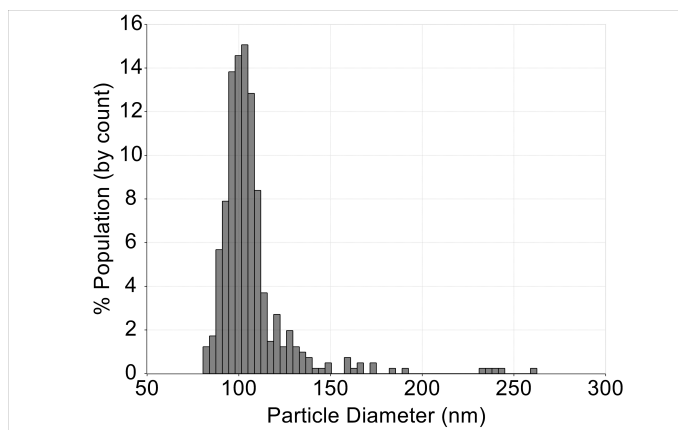
540

Figure S5: Size distribution histogram for the 8% sample at a shear rate of 121×10^3 s^{-1}. The

particle count for this sample was 405.

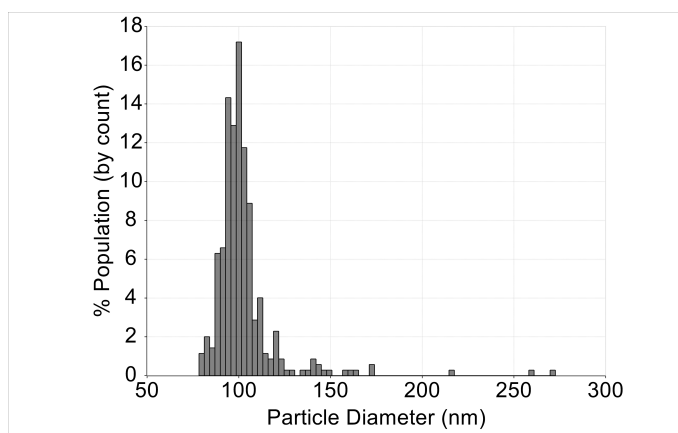**Figure S6:** Size distribution histogram for the 8% sample at a shear rate of 258×10^3 s^{-1}. The
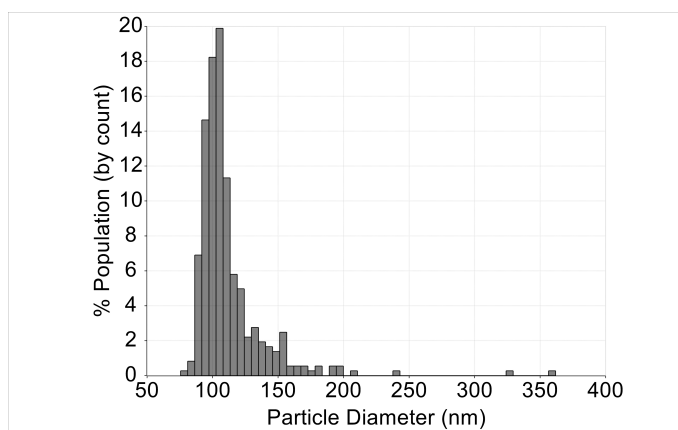
545   particle count for this sample was 349.

Figure S7: Size distribution histogram for the 8% sample at a shear rate of 686×10^3 s^{-1}. The

particle count for this sample was 307.

Table S1: Mean particle size for all excipient solutions as measured using the qViro-X technique. The adenovirus control had a mean particle diameter of 99 ± 17 nm and the deactivated adenovirus sample had a mean particle diameter of 113 ± 28 nm.

Shear rate ($\times 10^3$ s^{-1})	Mean particle diameter for 4% formulation (nm)	Mode particle diameter for 4% formulation (nm)	Mean particle diameter for 8% formulation (nm)	Mode particle diameter for 8% formulation (nm)
"no shear"	104 ± 27	93	103 ± 18	101
121	105 ± 26	94	107 ± 22	100
258	-	-	103 ± 19	103
391	101 ± 21	98	-	-
686	101 ± 21	97	106 ± 20	95

References

[1]   S. Ohtake *et al.*, "Heat-stable measles vaccine produced by spray drying," *Vaccine*, vol. 28, no. 5, pp. 1275–1284, 2010.

[2]   E. A. Corbanie, J. P. Remon, K. Van Reeth, W. J. M. Landman, J. H. H. Van Eck, and C. Vervaet, "Spray drying of an attenuated live Newcastle disease vaccine virus intended for respiratory mass vaccination of poultry," *Vaccine*, vol. 25, pp. 8306–8317, 2007.

560 [3] D. A. LeClair, L. Li, N. Rahman, E. D. Cranston, and M. R. Thompson, "Stabilization of HSV-2 viral vaccine candidate by spray drying," *Int. J. Pharm.*, vol. 569, no. May, p. 118615, 2019.

[4] D. A. LeClair, E. D. Cranston, Z. Xing, and M. R. Thompson, "Evaluation of excipients for enhanced thermal stabilization of a human type 5 adenoviral vector through spray
565 drying," *Int. J. Pharm.*, vol. 506, no. 1–2, pp. 289–301, 2016.

[5] N. Grasmeijer, "Improving protein stabilization by spray drying: formulation and process development," University of Groningen, 2016.

[6] V. Saluja, J.-P. Amorij, J. C. Kapteyn, A. H. de Boer, H. W. Frijlink, and W. L. J. Hinrichs, "A comparison between spray drying and spray freeze drying to produce an
570 influenza subunit vaccine powder for inhalation," *J. Control. Release*, vol. 144, no. 2, pp. 127–133, Jun. 2010.

[7] Y.-F. Maa and C. C. Hsu, "Effect of high shear on proteins," *Biotechnol. Bioeng.*, vol. 51, no. 4, pp. 458–465, 1996.

[8] J. Perdana, M. B. Fox, M. A. I. Schutyser, and R. M. Boom, "Enzyme inactivation
575 kinetics: Coupled effects of temperature and moisture content," *Food Chem.*, vol. 133, no. 1, pp. 116–123, 2012.

[9] A. Ghandi, I. B. Powell, T. Howes, X. D. Chen, and B. Adhikari, "Effect of shear rate and oxygen stresses on the survival of Lactococcus lactis during the atomization and drying stages of spray drying: A laboratory and pilot scale study," *J. Food Eng.*, vol. 113, no. 2,
580 pp. 194–200, 2012.

[10] D. A. LeClair, E. D. Cranston, Z. Xing, and M. R. Thompson, "Optimization of Spray Drying Conditions for Yield, Particle Size and Biological Activity of Thermally Stable Viral Vectors," *Pharm. Res.*, vol. 33, no. 11, pp. 2763–2776, 2016.

[11] B. A. Morgan, Z. Xing, E. D. Cranston, and M. R. Thompson, "Acoustic levitation as a screening method for excipient selection in the development of dry powder vaccines," *Int. J. Pharm.*, vol. 563, no. March, pp. 71–78, 2019.

[12] P. He, S. S. Davis, and L. Illum, "Chitosan microspheres prepared by spray drying.," *Int. J. Pharm.*, vol. 187, no. 1, pp. 53–65, 1999.

[13] P. Gong *et al.*, "Injury Mechanisms of Lactic Acid Bacteria Starter Cultures During Spray Drying : A Review," *Dry. Technol.*, vol. 32, pp. 793–800, 2014.

[14] B. C. S. To and M. R. Etzel, "Survival of Brevibacterium linens (ATCC 9174) after Spray Drying , Freeze Drying , or Freezing," *J. Food Sci.*, vol. 62, no. 1, pp. 167–170, 1997.

[15] M. S. Levy, I. J. Collins, S. S. Yim, J. M. Ward, P. A. Shamlou, and P. Dunnill, "Effect of shear on plasmid DNA in solution," *Bioprocess Eng.*, vol. 20, pp. 7–13, 1999.

[16] Y. F. Maa and C. C. Hsu, "Protein denaturation by combined effect of shear and air-liquid interface.," *Biotechnol. Bioeng.*, vol. 54, no. 6, pp. 503–12, 1997.

[17] R. Michalsky, P. H. Pfromm, P. Czermak, C. M. Sorensen, and A. L. Passarelli, "Effects of temperature and shear force on infectivity of the baculovirus Autographa californica M nucleopolyhedrovirus," *J. Virol. Methods*, vol. 153, pp. 90–96, 2008.

[18] D. H. D'Souza, X. Su, A. Roach, and F. Harte, "High-Pressure Homogenization for the

585

590

595

600

Inactivation of Human Enteric Virus Surrogates," *J. Food Prot.*, vol. 72, no. 11, pp. 2418–2422, 2009.

[19] J. Wang *et al.*, "Single Mucosal, but Not Parenteral, Immunization with Recombinant Adenoviral-Based Vaccine Provides Potent Protection from Pulmonary Tuberculosis," *J. Immunol.*, vol. 173, no. 10, pp. 6357–6365, 2004.

[20] E. K. Roediger, K. Kugathasan, X. Z. Zhang, B. D. Lichty, and Z. Xing, "Heterologous boosting of recombinant adenoviral prime immunization with a novel vesicular stomatitis virus-vectored tuberculosis vaccine," *Mol. Ther.*, vol. 16, no. 6, pp. 1161–1169, 2008.

[21] S. P. Toniolo *et al.*, "Excipient selection for thermally stable enveloped and non-enveloped viral vaccine platforms in dry powders," *Int. J. Pharm.*, vol. 561, no. January, pp. 66–73, 2019.

[22] M. R. Thompson, Z. Xing, D. A. LeClair, and E. D. Cranston, "Enhanced thermal stability for adenoviral vectors through spray drying," US20190062692A1, 2019.

[23] P. D. Hede, P. Bach, and A. D. Jensen, "Two-fluid spray atomisation and pneumatic nozzles for fluid bed coating / agglomeration purposes : A review," *Chem. Eng. Sci.*, vol. 63, pp. 3821–3842, 2008.

[24] H. Rumpf, "The strength of granules and agglomerates," *Agglom. First Int. Symp. Agglom. Philadelphia, 1962*, pp. 379–418, 1962.

[25] C. Zaiontz, "Real Statistics Resource Pack (Release 6.2)." 2019.

[26] M. B. Appaiahgari and S. Vrati, "Adenoviruses as gene/vaccine delivery vectors: promises and pitfalls," *Expert Opin. Biol. Ther.*, vol. 15, no. 3, pp. 337–351, 2015.

[27] M. O. Lasaro and H. C. J. Ertl, "New insights on adenovirus as vaccine vectors," *Mol. Ther.*, vol. 17, no. 8, pp. 1333–1339, 2009.

625 [28] A. C. Eischeid, J. N. Meyer, and K. G. Linden, "UV disinfection of adenoviruses: Molecular indications of DNA damage efficiency," *Appl. Environ. Microbiol.*, vol. 75, no. 1, pp. 23–28, 2009.

[29] S. E. Beck, N. M. Hull, C. Poepping, and K. G. Linden, "Wavelength-dependent damage to adenoviral proteins across the germicidal UV spectrum," *Environ. Sci. Technol.*, vol. 630 52, no. 1, pp. 223–229, 2018.

[30] R. Vogel *et al.*, "Quantitative Sizing of Nano/Microparticles with a Tunable Elastomeric Pore Sensor," *Anal. Chem.*, vol. 83, pp. 3499–3506, 2011.

[31] M. A. Kennedy and R. J. Parks, "Adenovirus virion stability and the viral genome: Size matters," *Mol. Ther.*, vol. 17, no. 10, pp. 1664–1666, 2009.

635 [32] L. L. Bondoc Jr. and S. Fitzpatrick, "Size distribution analysis of recombinant adenovirus using disc centrifugation," *J. Ind. Microbiol. Biotechnol.*, vol. 20, pp. 317–322, 1998.

[33] S. A. Berkowitz and J. S. Philo, "Monitoring the homogeneity of adenovirus preparations (a gene therapy delivery system) using analytical ultracentrifugation," *Anal. Biochem.*, vol. 362, pp. 16–37, 2007.

640 [34] M. McEvoy, V. Razinkov, Z. Wei, J. R. Casas-Finet, G. I. Tous, and M. A. Schenerman, "Improved Particle Counting and Size Distribution Determination of Aggregated Virus Populations by Asymmetric Flow Field-Flow Fractionation and Multiangle Light Scattering Techniques," *Biotechnol. Prog.*, vol. 27, no. 2, pp. 547–554, 2011.

[35]   J. Rexroad, R. K. Evans, and C. R. Middaugh, "Effect of pH and ionic strength on the physical stability of adenovirus type 5," *J. Pharm. Sci.*, vol. 95, no. 2, pp. 237–247, 2006.

[36]   J. C. Flesch, P. T. Spicer, and S. E. Pratsinis, "Laminar and turbulent shear-induced flocculation of fractal aggregates," *AIChE J.*, vol. 45, no. 5, pp. 1114–1124, 1999.

[37]   P. Meakin, "Fractal aggregates," *Adv. Colloid Interface Sci.*, vol. 28, pp. 249–331, 1987.

[38]   T. M. Dobrowsky *et al.*, "Adhesion and fusion efficiencies of human immunodeficiency virus type 1 (HIV-1) surface proteins," *Sci. Rep.*, vol. 3, pp. 1–9, 2013.

645

650